ACS Partner Journal

ACCOUNTS of materials research

pubs.acs.org/amrcda

Article

From Understanding of Catalyst Functioning toward Controlling Selectivity in CO_2 Hydrogenation to Higher Hydrocarbons over Fe-Based Catalysts

Qingxin Yang* and Evgenii V. Kondratenko*

Cite This: https://doi.org/10.1021/accountsmr.4c00160

Read Online

ACCESS | Metrics & More | Article Recommendations

CONSPECTUS: The conversion of carbon dioxide (CO_2) with hydrogen (H_2), generated by renewable energy sources, into value-added products is a promising approach to meet future demands for sustainable development. In this context, the hydrogenation of CO_2 (CO_2-FTS) to higher hydrocarbons (C_{2+}), lower olefins, and fuels should be mentioned in particular. These products are used in our daily lives but are currently produced by energy-intensive and CO_2-emitting oil-based cracking processes. The environmental compatibility and abundance of iron (Fe) used in CO_2-FTS catalysts are also relevant to sustainable development. The CO_2-FTS reaction was inspired by the experience accumulated in long-term research on Fischer−Tropsch synthesis with CO (CO-FTS). A simple grafting of catalyst formulations and reaction mechanisms from CO-FTS to CO_2-FTS has, however, been proven unsatisfactory, likely due to differences in surface adsorbates, chemical potentials of CO and CO_2, and H_2O partial pressure. These characteristics affect both the catalyst structure and the reaction pathways. Consequently, CO_2-FTS provides higher CH_4 selectivity but lower C_{2+}-selectivity than does CO-FTS, which appeals to fundamental research to hinder CH_4 formation.

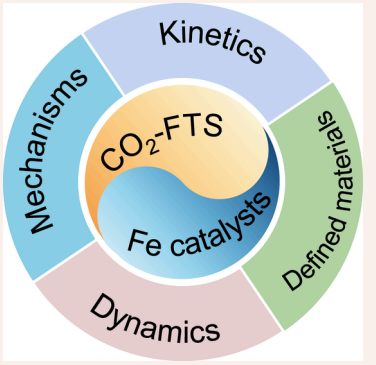

In this Account, our recent progress in identifying descriptors for purposeful catalyst design is highlighted. Different from the trial-and-error methods and chemist's intuition strategies commonly used for catalyst design, our initial efforts were devoted to a meta-analysis of literature data to identify catalyst property−performance relationships in CO_2-FTS. The resulting hypotheses were experimentally validated and provided the basis for catalyst development. Our other distinguishing strategy is spatially resolved analyses of reaction-induced catalyst restructuring and reaction kinetics. As the catalyst composition changes downstream of the catalyst bed, it is critical to consider the respective profiles to establish proper correlations between the working catalyst phase and species and the kinetics of the formation of selective and unselective reaction products. The importance of in situ characterization studies for understanding reaction-induced catalyst restructuring is especially highlighted. We also demonstrate the power of transient kinetic methods, i.e., temporal analysis of products (TAP) and steady-state isotopic transient kinetic analysis (SSITKA), to identify the mechanism and microkinetics of the activation of CO_2, CO, and H_2 that characterize the efficiency of iron carbides for CO_2 hydrogenation. The SSITKA method is also instrumental in quantifying the abundance and lifetime of surface intermediates, leading to CO or CH_4. The global network of product formation is further established by analyzing selectivity−conversion relationships to identify primary and secondary products. Our spatially and time-resolved analyses of catalyst composition and product formation rates can be useful for various heterogeneous reactions studied in plug flow reactors because the partial pressures of feed components and reaction products change along the catalyst bed. Such changes can result in spatial profiles of active phases/species. Combining catalyst structural features with kinetic/mechanistic information allowed us to elucidate the fundamentals of controlling catalyst activity and product selectivity and the mechanism of catalyst deactivation. We also present how the derived knowledge aids in the design of robust Fe-based catalysts, paving the way for the current studies one step closer to the implementation of more sustainable CO_2 utilization.

1. INTRODUCTION

To meet the principles of sustainable and circular economy, the chemical industry is undergoing a grand transition in modern production and energy storage scenarios. In this context, catalysis will continue to play a crucial role, relying heavily on the targeted development of efficient catalysts. Benefiting from the low cost, environmental friendliness, and earth-abundance of iron (Fe), Fe-based catalysts have found application in many

Received: May 20, 2024
Revised: August 21, 2024
Accepted: September 3, 2024

reactions. Inspired by Fe-containing hydrogenase enzymes in nature, iron complexes have been successfully used as homogeneous catalysts for organic synthesis.[1] Solid Fe-based catalysts in the form of both supported and bulk oxides, carbides, or metal, have attractive potential in numerous industrial processes.[2,3] Despite decades of research, the determination of structure−function relationships of Fe-constituted active sites, species, and phases remains challenging. In this regard, the motivation to investigate Fe-based catalysts is compelling from both fundamental research and practical application perspectives. However, it is beyond the scope of this contribution to provide a comprehensive overview of the properties and catalytic functions of Fe-based materials, which are discussed in previous dedicated reviews.[4,5]

Herein, we focus on the direct synthesis of C_{2+}-hydrocarbons (lower olefins and liquid fuels) by thermocatalytic CO_2 hydrogenation, also known as CO_2-based Fischer−Tropsch synthesis (CO_2-FTS),[6,7] over Fe-based catalysts. This reaction represents a promising approach to closing the carbon cycle, when H_2 is produced on a CO_2-free basis, and alleviates our dependence on oil-based processes. Early studies of CO_2-FTS have shown that cobalt-based catalysts suffer from excessive CH_4 production,[8] while Fe-based catalysts allow the formation of C_{2+}-hydrocarbons as illustrated in Scheme 1.[7,9] However, the

Scheme 1. Overall Network of Product Formation in CO_2-FTS over Fe-Based Catalysts

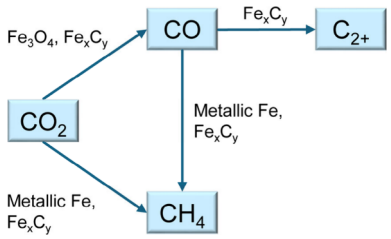

coproduction of CH_4 has precluded the commercialization of CO_2-FTS process(es) and has, therefore, triggered a growing interest in the development of more selective catalysts. Rational catalyst design is hampered by insufficient knowledge of catalyst functioning due to the complexity of Fe-based catalysts. Their working composition is generated in situ and depends on the ability of iron oxides, metallic iron, and iron carbides (Fe_xC_y) to react with reducing (CO/H_2/hydrocarbons) and oxidizing (CO_2/H_2O) agents.[10,11] Iron carbides are accepted to be involved in the formation of the desired products.[2,9] They also contribute to the formation of CH_4 and CO.[12]

Especially, we demonstrate the advantages of the controlled synthesis of Fe-containing materials composed of specific phases to analyze their changes under CO_2-FTS conditions in a spatially resolved manner. Combined with spatially and temporally resolved kinetic analysis of product formation, this structural information is instrumental in establishing structure−performance relationship(s) relevant for targeted catalyst design. The usefulness of a meta-analysis of literature data to identify catalyst property−performance relationships in the CO_2-FTS is also discussed. The impact of the developed catalysts is demonstrated by the comparison with state-of-the-art catalysts. Future opportunities and remaining challenges in CO_2-FTS are also identified.

2. DATA-DRIVEN APPROACHES FOR TARGETED CATALYST DESIGN

Interest in the application of data science and machine learning to targeted catalyst design has recently increased and shows great potential to overturn the traditional trial-and-error paradigm for preparing heterogeneous catalysts.[13,14] In this context, the pioneering work of Zavyalova et al.[15] should be mentioned, which used statistical analysis of literature data to establish correlations between catalyst composition and performance in the oxidative coupling of methane. Motivated by this study, our group has demonstrated the potential of regression trees and multiway analysis of variance (ANOVA) methods to identify the key descriptors affecting catalyst performance in CO_2-FTS (Figure 1a).[16] The outcome of our study has stimulated other research groups working on this reaction to further study in this direction.[17,18] The target performance metrics in our study include the rates of CO_2 conversion and C_{2+} formation, the selectivity to C_{2+}-hydrocarbons ($S(C_{2+})$), and the molar ratio of lower olefins to lower paraffins ($O(C_2{-}C_4)/P(C_2{-}C_4)$). We considered only articles that contain quantitative catalyst composition, complete performance data, and fully described reaction conditions. Among the first-group descriptors (kind of catalyst, physicochemical properties, and reaction conditions), the use of bulk and promoted catalysts (Cat. kind: 2 in Figure 1b) was identified as the most decisive descriptor influencing the selectivity to C_{2+}-hydrocarbons.

Given the pivotal role of promoters, the second group of descriptors that includes the kind of promoter were tested for their significance on the above performance metrics. Sodium was found to be the most important promoter in determining $S(C_{2+})$ (Figure 1c). Furthermore, the combination of Na with Mn should additionally increase this performance. The multiway ANOVA analyses further showed a particularly high statistical significance ($p < 0.000002$) regarding the decisive effect of Na on $S(C_{2+})$ and $O(C_2{-}C_4)/P(C_2{-}C_4)$.[16] In contrast to their positive influence on the selectivity of the desired products, alkali promoters do not impose a positive effect on the CO_2 conversion rate. In addition, we have successfully correlated the statistically average values of methane selectivity with the electronegativity of the promoter element used.[16] The fundamentals of the established effects of alkali metal promoters are discussed in detail in Sections 4 and 5.

Guided by the findings of our meta-analysis, we prepared a series of bulk Fe_2O_3 catalysts promoted by oxides of K, Mn, or K and Mn. The predicted synergistic effect between these two promoters was confirmed. The highest $S(C_{2+})$ of around 83% at 42% CO_2 conversion was obtained over the optimal catalyst (0.04Mn-K/Fe) at 300 °C and 15 bar. This performance is remarkable when compared to that of previously developed state-of-the-art catalysts (Figure 1d). This strategy of combining an alkali metal and a transition metal as promoters for Fe-based catalysts has been further reported in the following works.[21] By adopting a precise synthesis procedure and modulating the key physicochemical properties of FeO_x without any promoter, we were further able to lower the selectivity to methane (Figure 1e and Section 3.1) or to practically completely suppress the formation of all hydrocarbons in favor of CO (Figure 1f and Section 3.2).

https://doi.org/10.1021/accountsmr.4c00160
Acc. Mater. Res. XXXX, XXX, XXX−XXX

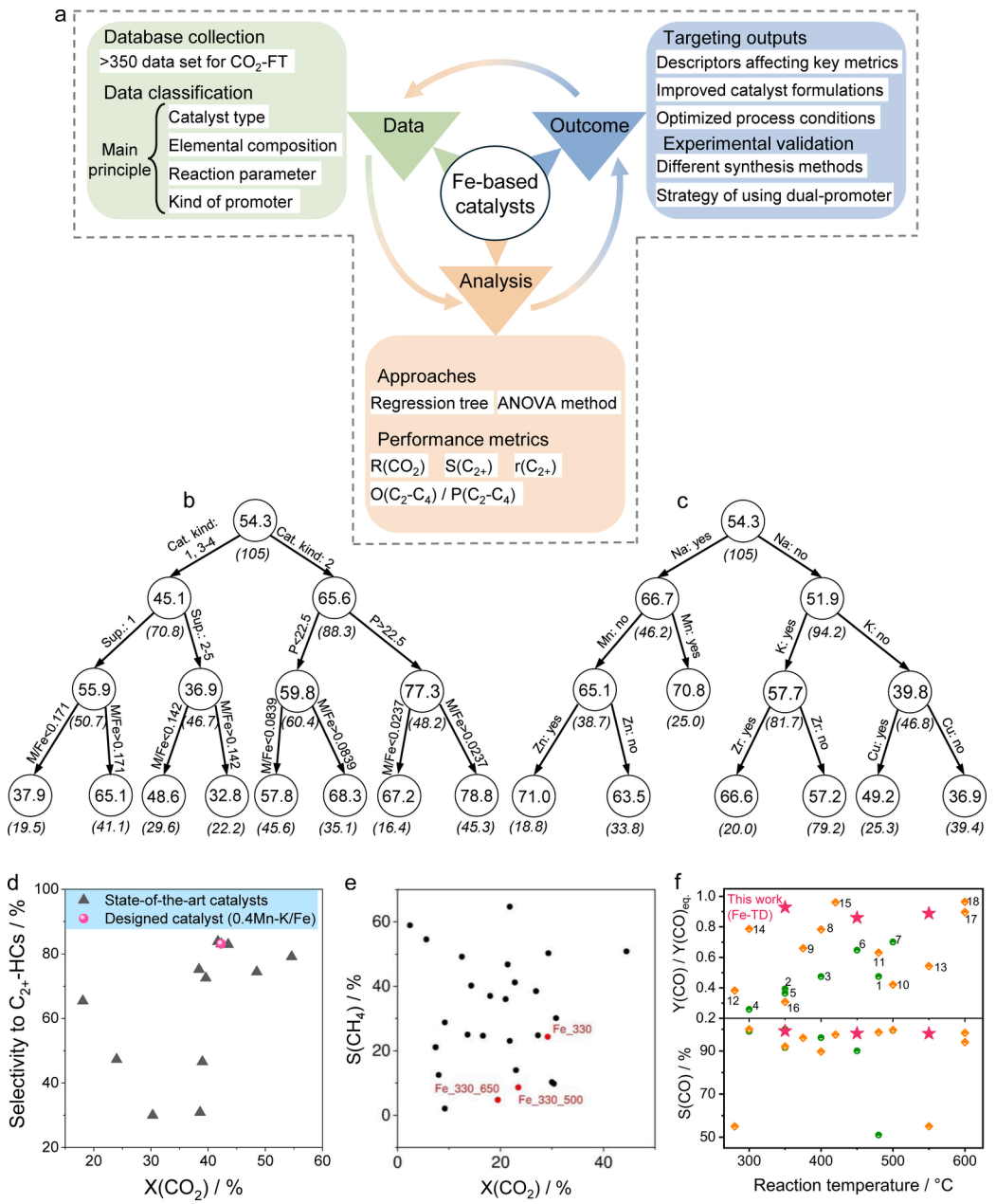

Figure 1. Data-driven approach for catalyst design. (a) Illustration of meta-analysis of collected literature data. (b–c) Regression trees of $S(C_{2+})$ based on (b) the first-group descriptors and (c) the second-group descriptors. Each node is labeled with the mean value of this performance. Decoding of catalyst kind (Cat. kind) and support material (Sup.) is given in ref 16. Reproduced with permission from ref 16. Copyright 2021 Elsevier. (d) Comparison of the developed catalyst 0.4Mn-K/Fe with other state-of-the-art catalysts reported in the literature in terms of $S(C_{2+})$ and $X(CO_2)$. (e) $S(CH_4)$ obtained over iron oxalate-derived catalysts (red dots) and reported bulk and unpromoted Fe-based catalysts (black dots). Reproduced with permission from ref 19. Copyright 2021 Elsevier. (f) CO selectivity and the $Y(CO)/Y(CO)_{eq}$ ratio were obtained over Fe-TD and state-of-the-art catalysts at different temperatures. Reproduced with permission from ref 20. Copyright 2023 Elsevier.

3. STRATEGIES FOR PREPARATION OF WELL-DEFINED FE-BASED CATALYSTS AND THEIR PERFORMANCE IN CO_2 HYDROGENATION

Since iron carbides (Fe_xC_y) are the active components involved in the formation of C_{2+}-hydrocarbons in CO_2-FTS but are typically formed in situ or ex situ from different Fe-containing compounds, it is highly important to understand these phase transformations to control product selectivity. As concluded from our meta-analysis[16] (Figure 1) and a recent experimental study using bulk Fe-Al-Cu-K and supported Fe-K-Cu/Al_2O_3 catalysts,[22] bulk Fe-based catalysts appear to be more efficient than their supported counterparts but may suffer from low mechanical stability and carbon fouling. These factors may cause the disintegration of catalyst particles and/or catalyst deactivation in CO/CO_2-FTS. Therefore, supported Fe-based catalysts have also been developed for CO_2-FTS.[23−25] Suitable supports can also participate in the activation of reactants, thus providing a synergistic effect on the catalytic performance with Fe-containing phases together. Various approaches are used to prepare supported and bulk Fe-containing catalysts with specific structural properties (Figure 2a).[26,27] Some representative results are presented and discussed in the below sections.

https://doi.org/10.1021/accountsmr.4c00160
Acc. Mater. Res. XXXX, XXX, XXX−XXX

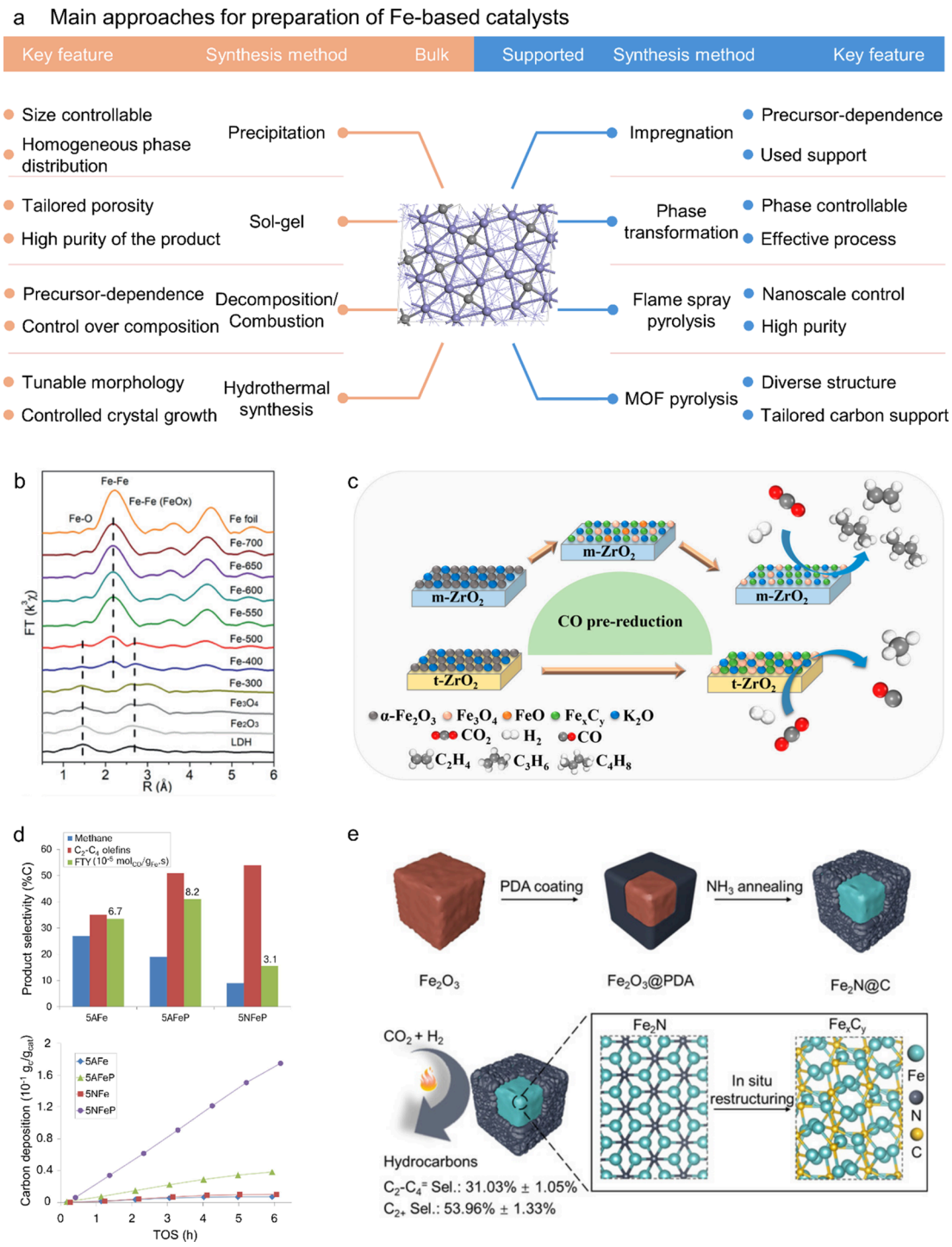

Figure 2. Synthesis of bulk or supported Fe-based catalysts and catalytic performance of the latter. (a) Summary of representative methods for the preparation of bulk and supported Fe-based catalysts. (b) K-edge extended X-ray absorption fine structure (EXAFS) of the MgFeAl-LDH material and LDH-derived catalysts. Reproduced with permission from ref 24. Copyright 2021 Wiley-VCH. (c) Phase transformations of m-ZrO_2- or t-ZrO_2-supported Fe-containing catalysts during CO pretreatment. Reproduced with permission from ref 25. Copyright 2021 American Chemical Society. (d) CH_4 and C_2-C_4 olefins selectivity and iron-related space time yield of CO conversion as well as the level of carbon deposition in CO-FTS over Fe/α-Al_2O_3 prepared with ammonium iron citrate as precursor (5AFe and 5AFeP) or with iron nitrate as precursor (5NFeP). Reproduced with permission from ref 23. Copyright 2013 Elsevier. (e) The preparation of Fe_2N material and its reconstruction to Fe_xC_y in CO_2-FTS. Reproduced with permission from ref 30. Copyright 2021 Wiley-VCH.

3.1. Supported Fe-Based Catalysts

Impregnation of a support material with a solution of an Fe-containing salt is still the most commonly used method for the preparation of technical catalysts.[28] Both the type of Fe-containing precursor and support material and catalyst treatment conditions influence the physicochemical properties of the resulting phases. For example, the CO-induced carburization of FeO_x species/phases on the surface of monoclinic ZrO_2 to Fe_5C_2 was found to occur via FeO as an intermediate phase due to the strong interaction between the Fe-containing species/

https://doi.org/10.1021/accountsmr.4c00160
Acc. Mater. Res. XXXX, XXX, XXX−XXX

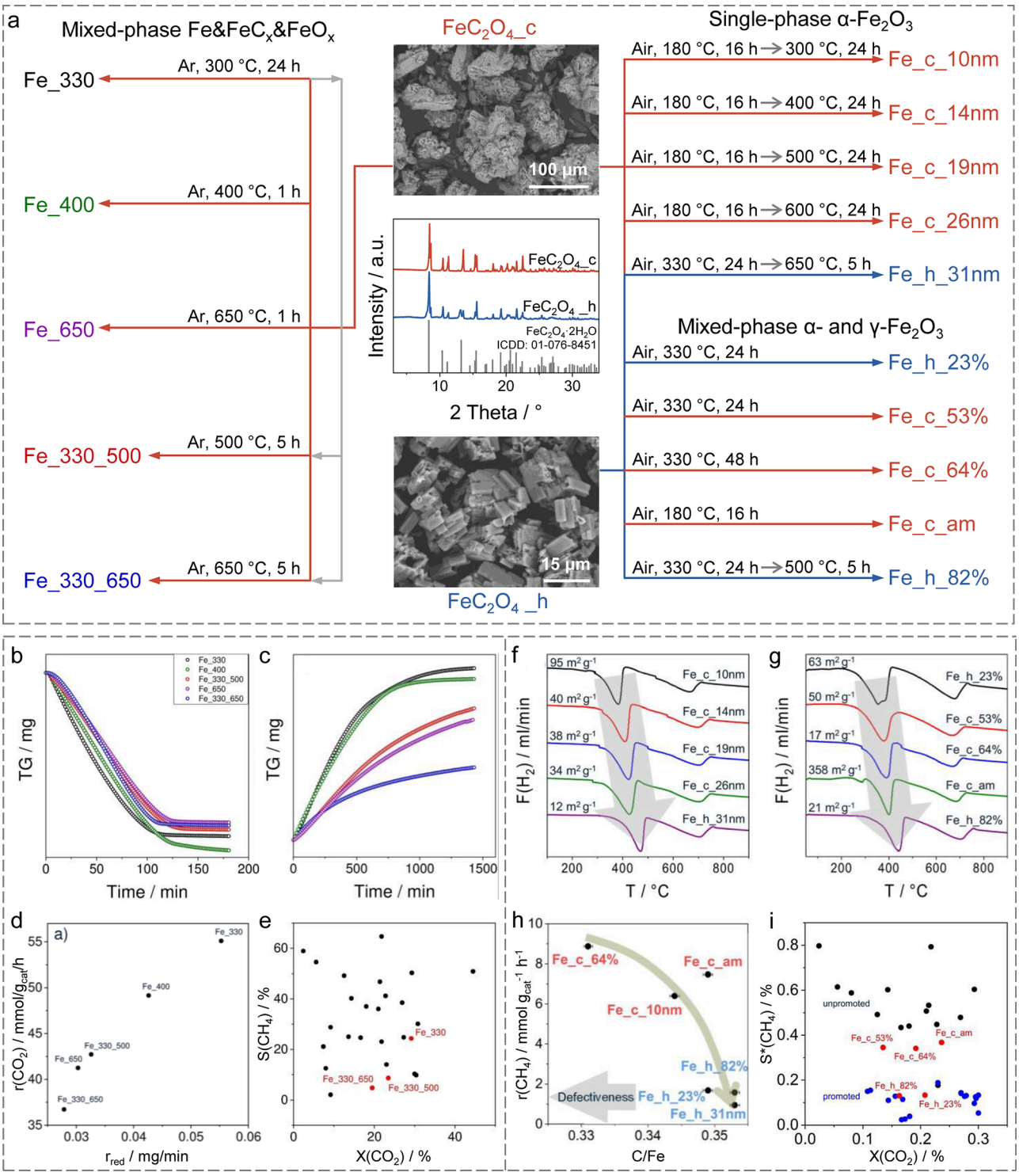

Figure 3. Bulk Fe-based catalysts prepared by decomposition of $FeC_2O_4{\cdot}2H_2O$. (a) Scheme showing the preparation procedure of Fe-based materials through decomposition of commercial or homemade $FeC_2O_4{\cdot}2H_2O$, including their presentative scanning electron microscope (SEM) images and X-ray diffraction (XRD) patterns. Accordingly, the resulting materials are abbreviated as "Fe_c_" and "Fe_h_", while the ending codes "x nm" and "y%" represent the crystallite size of single-phase α-Fe_2O_3 and the weight fraction of α-Fe_2O_3 in mixed-phase catalysts, respectively. (b, c) TGA profiles of $Fe_xO_yC_z$ samples upon (b) reduction in H_2 and (c) the following reoxidation in CO_2. (d) The effect of the reduction rate of the $Fe_xO_yC_z$ catalysts on the CO_2 consumption rate in CO_2-FTS. (e) $S(CH_4)$ over the $Fe_xO_yC_z$ catalysts (red dots) and previously reported bulk and unpromoted Fe-based catalyst (black dots). Reproduced with permission from ref 19. Copyright 2021 Elsevier. (f, g) Profiles of H_2 flow upon H_2-TPR of catalysts initially consisting of (f) a single α-Fe_2O_3 phase or (g) mixed α-/γ- Fe_2O_3 phases. (h) The effect of the C/Fe ratio in Fe_5C_2 on the rate of methane formation in CO_2-FTS. (i) CH_4 selectivity (excluding CO) over in-house synthesized catalysts (red dots) and previously reported unpromoted (black dots) or promoted bulk (blue dots) Fe-based catalysts. Reproduced with permission from ref 34. Copyright 2022 American Chemical Society.

phases and monoclinic ZrO_2, lowering the carburization rate compared to the catalyst based on tetragonal ZrO_2 (Figure 2c).[25] The slower the rate, the smaller the size of the Fe_5C_2 particles. Barrios et al.[29] prepared a series of ZrO_2-supported Fe-

https://doi.org/10.1021/accountsmr.4c00160
Acc. Mater. Res. XXXX, XXX, XXX−XXX

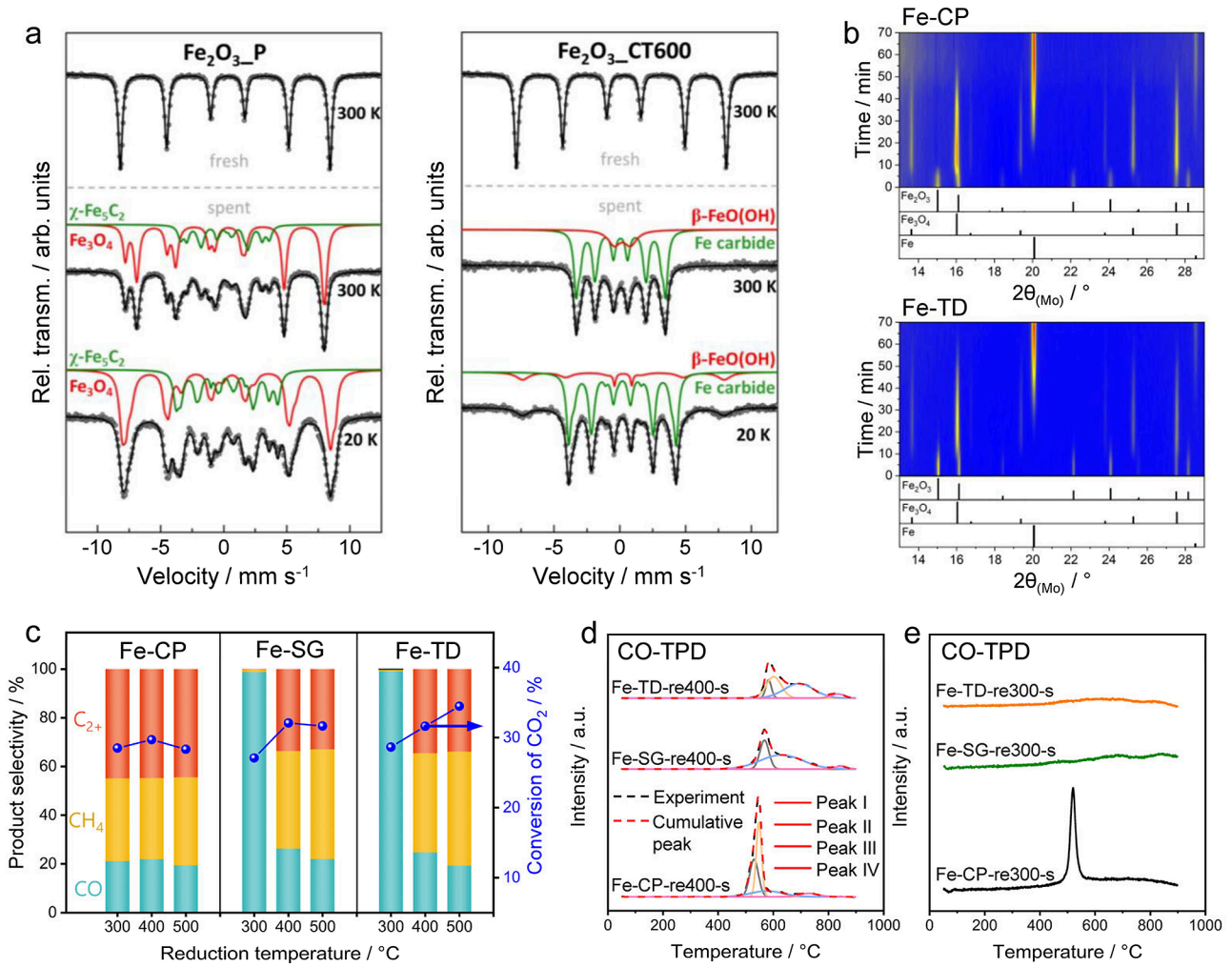

Figure 4. Bulk Fe-based catalysts prepared with iron nitrate as precursor. (a) Mössbauer spectra of fresh Fe-based catalysts and their spent counterparts after CO_2-FTS. Reproduced with permission from ref 36. Copyright 2017 Elsevier. (b) Heatmap of in situ XRD profiles obtained during the reductive treatment of Fe-CP and Fe-TD. (c) The effects of catalyst reduction temperature before CO_2-FTS on CO_2 conversion and product selectivity over Fe-CP, Fe-SG, and Fe-TD at 350 °C and 15 bar (CO_2:H_2:N_2 = 1/3/0.3). (d, e) Temperature-programmed desorption profiles of CO of spent catalysts prereduced at (d) 400 °C or (e) 300 °C before CO_2-FTS. Reproduced with permission from ref 20. Copyright 2023 Elsevier.

based catalysts with different promoters to elucidate their role in CO_2-FTS. In agreement with our meta-analysis,[16] it was concluded that the combination of potassium with another promoter (Cs, Mo, Cu, Ga, or Ce) is a promising strategy for the design of catalysts with high selectivity to light olefins. The promoters influence iron dispersion and carburization, as well as catalyst basicity.

The phase transformation of Fe-containing layered double hydroxide (LDH) materials represents an effective approach for the synthesis of supported catalysts with a tunable composition. The oxidation state of Fe in the LDH-derived Fe/MgO-Al_2O_3 catalysts depends on the treatment temperature (300−700 °C) of the MgFeAl-LDH nanosheets (Figure 2b).[24] A moderate temperature of 500 °C resulted in a highly active catalyst (Fe-500) that displays a C_{2+}-selectivity of 53% at 50% CO_2 conversion in photothermal CO_2 hydrogenation.

To achieve a homogeneous distribution of iron carbides on a support, de Jong et al.[23] used ammonium iron citrate as a precursor for impregnation of Al_2O_3. The resulting catalyst (5AFeP) showed a higher activity in CO-FTS (iron time yield, FTY) than the catalyst (5NFeP) prepared with iron nitrate (Figure 2d). Moreover, a higher level of carbon deposition was determined for the latter catalyst.

Catalysts based on carbon supports with confined FeO_x species have received increasing attention due to the tailorable surface properties and appropriate mechanical strength of the support materials. These catalysts can be prepared by conventional impregnation of various carbonaceous materials or by pyrolysis of metal−organic framework (MOF) materials.[31] Zhao et al.[30] recently developed a method to prepare iron carbides (Fe_xC_y@C) from carbon-wrapped iron nitride (Fe_2N@C) (Figure 2e). The resulting Fe_xC_y@C catalyst displayed 31% selectivity to lower olefins (CO-free basis) at 34% CO_2 conversion in the CO_2-FTS reaction at 250 °C and 10 bar.

3.2. Bulk Fe-Based Catalysts

From a fundamental point of view, our efforts have been focused on tuning the reducibility of iron oxides to verify if and how this material property influences the formation of iron carbides and their structural properties, which could bring distinctive performance in CO_2-FTS. In general, the reducibility of metal oxides can be controlled by constructing interface(s) between supported metal and bulk oxide, by introducing metal dopant, or by optimizing the nanostructure of the bulk oxides.[32] To avoid

https://doi.org/10.1021/accountsmr.4c00160
Acc. Mater. Res. XXXX, XXX, XXX−XXX

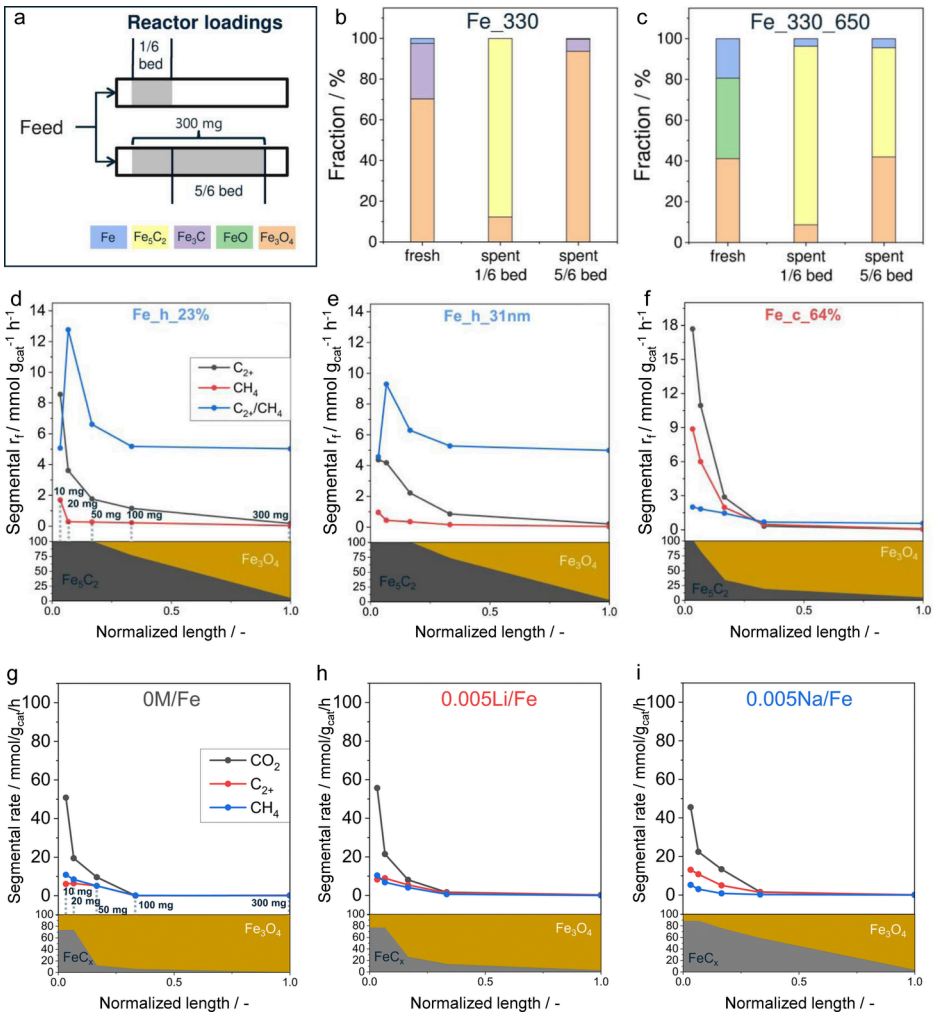

Figure 5. Spatially resolved analysis of Fe-containing phases and kinetics of product formation. (a) A scheme showing catalyst layer in a reactor. (b, c) Composition of fresh and spent (b) Fe_330 and (c) Fe_330_650 determined by the analysis of Mössbauer spectra. Reproduced with permission from ref 19. Copyright 2021 Elsevier. (d–i) Spatial distribution of Fe-containing phases along the catalyst bed and segmental rates of overall CO_2 consumption, C_{2+} formation, CH_4 formation, and the ratio of the two latter rates for (d) Fe_h_23%, (e) Fe_h_31 nm, (f) Fe_c_64%, (g) 0M/Fe, (h) 0.005Li/Fe, and (i) 0.005Na/Fe. The catalysts for (d–f) are shown in the right panel of Figure 3a. In (g–i), $FeC_2O_4{\cdot}2H_2O$ with or without alkali promoter was directly used as fresh catalysts. (d–f) Reproduced with permission from ref 34. Copyright 2022 American Chemical Society. (g–i) Reproduced from ref 37 with permission from The Royal Society of Chemistry.

any effects of a secondary metal for Fe-based catalysts, we focused on the latter method by controlling the dimensionality, composition, and morphology of iron oxides. To this end, various iron oxides were prepared from either iron(II) oxalate dihydrate ($FeC_2O_4{\cdot}2H_2O$ in Section 3.2.1) or iron(III) nitrate (Section 3.2.2) with different procedures or synthetic methods.

3.2.1. Controlled Decomposition of Iron(II) Oxalate. $FeC_2O_4{\cdot}2H_2O$ serves as a suitable platform for the synthesis of Fe-containing materials with tunable composition.[33] For example, its decomposition in Ar results in materials consisting of iron oxides, carbides, and metallic iron, which are referred to in this manuscript as $Fe_xO_yC_z$ (left panel in Figure 3a).[19] The exact composition depends on the decomposition temperature/duration and determines the redox properties of $Fe_xO_yC_z$ materials as demonstrated by thermogravimetric analysis (TGA), using H_2 and CO_2 as reducing and oxidizing agents, respectively. The highest reduction rate was determined for Fe_330, which has Fe_3O_4 with the smallest crystallites (Figure 3b). Metallic Fe formed during this reduction process can be reoxidized with CO_2 (Figure 3c). The rate of this process correlates with the size of metallic Fe crystallites.

Interestingly, the CO_2 consumption rate in CO_2-FTS over the $Fe_xO_yC_z$ materials is positively correlated with the rate of their reduction (Figure 3d). As the RWGS reaction over FeO_x catalysts (i.e., the first step of CO_2-FTS) is widely reported to follow the redox mechanism,[35] the high rate of lattice oxygen removal from FeO_x may facilitate CO_2 conversion. Benefiting from the suppressed CO/CO_2 methanation activity, Fe_330_550 and Fe_330_650 displayed low CH_4 selectivity compared with unpromoted state-of-the-art catalysts (Figure 3e).

In contrast to the decomposition of $FeC_2O_4{\cdot}2H_2O$ in Ar, the decomposition of this material in air produced single-phase α-Fe_2O_3 or mixed-phase α-Fe_2O_3 and γ-Fe_2O_3 (right panel in Figure 3a).[34] The final composition is dependent on the calcination conditions applied. For the single-phase materials, H_2-TPR tests revealed that the temperature of the maximal rate of α-Fe_2O_3 reduction to Fe_3O_4 (T_{max}) increases with increasing size of α-Fe_2O_3 crystallites (Figure 3f). In the case of the mixed-

https://doi.org/10.1021/accountsmr.4c00160
Acc. Mater. Res. XXXX, XXX, XXX−XXX

phase catalysts, the higher the fraction of the γ-Fe_2O_3 phase, the lower the T_{max} (Figure 3g). This dependence was explained by the similarity of the crystal lattices of Fe_3O_4 and γ-Fe_2O_3. The structural and redox properties of Fe_2O_3 discussed above were established to be important for the defectiveness of Fe_5C_2 formed in situ in CO_2-FTS, defined as the C/Fe ratio determined by fitting Mössbauer spectra. Importantly, this ratio appears to be a descriptor relevant to the rate of CH_4 formation in the CO_2-FTS (Figure 3h). The defect-less Fe_5C_2 has a higher ability to activate CO and CO_2 with a limited ability to activate H_2. As a result, the Fe_h_* catalysts show much lower selectivity to methane compared to reported unpromoted Fe-based catalysts and even are comparable to promoted catalysts (Figure 3i).

3.2.2. Fe_2O_3 Prepared from Iron Nitrate. $Fe(NO_3)_3 \cdot 9H_2O$ is one of the most often used precursors to prepare iron oxides.[28] For example, α-Fe_2O_3 materials were prepared by using the cellulose-templated (Fe_2O_3_CT600) and precipitation (Fe_2O_3_P) methods.[36] Their H_2-TPR profiles revealed an easier reducibility of the former catalyst. The spent Fe_2O_3_CT600 after 120 h on stream contains about 80 wt % iron carbides higher than 30 wt % in the spent Fe_2O_3_P (Figure 4a). Consequently, the former catalyst achieved $S(C_{2+})$ of 65% at 40% CO_2 conversion, outperforming the latter and other reported state-of-the-art catalysts.[36]

The presence of iron carbides was not proven to be sufficient to produce C_{2+}-hydrocarbons.[20] α-Fe_2O_3-based catalysts were synthesized from $Fe(NO_3)_3 \cdot 9H_2O$ using precipitation (Fe-CP), sol–gel (Fe-SG), and thermal decomposition (Fe-TD) methods. In situ XRD measurements of catalyst reduction in H_2 showed that Fe_2O_3 is first reduced to Fe_3O_4, followed by the formation of metallic Fe (Figure 4b). These processes were accelerated as the crystallite size of Fe_2O_3 decreased.

The reduction temperature (300, 400, or 500 °C) of Fe-CP prior to CO_2-FTS was not found to affect the selectivity to CO and hydrocarbons (Figure 4c). These products were also formed over Fe-SG and Fe-TD prereduced at 400 or 500 °C. However, CO was formed exclusively over these materials prereduced at 300 °C. Although iron carbides were observed in all spent catalysts, their careful characterization by XRD and X-ray absorption spectroscopy revealed planar defects in Fe_5C_2 of spent Fe-CP and perfectly crystallized Fe_5C_2 of spent Fe-TD. Similar defects were also found in the iron sublattice of Fe_2O_3 in fresh Fe-CP.

On this basis it was concluded that the smaller the crystallite size of Fe_2O_3, the higher the reducibility and the higher the imperfection of Fe_5C_2 structure. The imperfection determines the formation of surface species from CO_2, CO, and H_2 (Figure 4d,e), which explains the different catalytic performance in CO_2-FTS. Importantly, CO adsorption was hardly observed over spent Fe-TD and Fe-SG prereduced at 300 °C.

4. SPATIALLY RESOLVED ANALYSIS OF FE-CONTAINING PHASES AND KINETICS OF PRODUCT FORMATION

Although there is no doubt that Fe_xC_y is formed in situ under CO_2-FTS conditions,[10,11] our studies[19,34,37] have demonstrated the need to control its spatial distribution for efficient production of the desired products (Figure 5). The uneven distribution of steady-state Fe-containing phases is caused by changes in the partial pressures of the reducing (H_2/CO/hydrocarbons) and oxidizing (CO_2/H_2O) reaction components along the catalyst bed, which contribute to the formation/oxidation of Fe_xC_y. Taking the Fe_330 and Fe_330_650 catalysts from Figure 3a as examples, it is obvious that their composition after CO_2-FTS depends on the position in the reactor (Figure 5a–c). Compared to the fresh catalysts, the fraction of Fe_3O_4 in the upstream 1/6 layer of their spent counterparts decreased strongly due to the formation of Fe_5C_2 in situ. While Fe_3O_4 was found to be the main phase in the downstream 5/6 layer of spent Fe_330 (Figure 5b), a significant fraction (50%) of Fe_5C_2 was identified in the downstream 5/6 layer of spent Fe_330_650. The difference between the catalysts is probably due to the easier carburization of FeO present in the fresh Fe_330_650 catalyst (Figure 5c). These results suggest that the differently prepared catalysts have different abilities to generate and stabilize Fe_xC_y. The redox properties and/or imperfection of Fe_2O_3 (Figure 3f–h) appear to influence the spatial distribution of Fe_5C_2 (Figure 5d–f).[34]

The presence and kind of alkali metal promoter is another factor affecting the spatial profiles of the steady-state Fe-containing phases in the catalysts synthesized by impregnation of $FeC_2O_4 \cdot 2H_2O$ with an aqueous solution of alkali-metal carbonate (Figure 5g–i).[37] For all catalysts, the fraction of Fe_5C_2 decreases downstream of the catalyst bed. However, the decrease is less pronounced for alkali-promoted catalysts, underscoring the role of the promoter in generating and/or stabilizing Fe_5C_2.[37] Furthermore, the surface concentration of Na in differently loaded Na/Fe_2O_3 catalysts was identified as a descriptor influencing the (un)steady-state catalyst composition under the fluctuating conditions of CO_2-FTS, i.e., the periodic removal of H_2 or CO_2 from the reaction feed.[38]

The discovery of the spatial distribution of Fe-containing phases motivated us to investigate the spatial kinetics of product formation. Since its inception in the work of Birtill,[39] the study with spatially resolved manner has been applied in catalysis research by our group and other researchers to analyze the changes in the rates of reactant conversion/product formation along the catalyst bed.[40,41] Such segmental rate analysis in CO_2-FTS could also explain the spatial distribution of Fe_xC_y because they are responsible for the formation of higher hydrocarbons[20,34,37,42] (Figure 5d–i). The rates determined in the first layer can also be used to compare the intrinsic activities of different catalysts due to differential reactor operation. In this regard, Fe_5C_2 formed in situ from Fe_c_64% shows the highest rate of C_{2+} formation ($r(C_{2+})$ in Figure 5d–f). Due to the transition from differential to integral reactor operation, the segmental $r(C_{2+})$ decreases downstream of the catalyst bed with the strongest decrease observed for Fe_c_64%. This difference can be explained by the greater ability of the Fe h-* catalysts to generate/stabilize Fe_5C_2. Moreover, Fe_c_64% displayed higher CH_4 formation rates in all segments in comparison to Fe_h_* catalysts. As a result, the ratio of $r(C_{2+})/r(CH_4)$ for Fe_h_* catalysts is much higher than that for Fe_c_64%, leading to low CH_4 selectivity over the former catalysts (Figure 3i).

The same approach was also applied to investigate the promoting effect of alkali metals on Fe_2O_3-based catalysts (M/Fe, M stands for alkali metal). In contrast to the unpromoted catalyst (0M/Fe) and 0.005Li/Fe, the production of C_{2+}-hydrocarbons was observed throughout the bed of 0.005Na/Fe (Figure 5g–i). The phase profile shows a higher FeC_x content especially in the downstream layer of 0.005Na/Fe (Figure 5i). Further, $r(CH_4)$ was higher than $r(C_{2+})$ in the first three segments of 0M/Fe (Figure 5g). However, the difference

https://doi.org/10.1021/accountsmr.4c00160
Acc. Mater. Res. XXXX, XXX, XXX–XXX

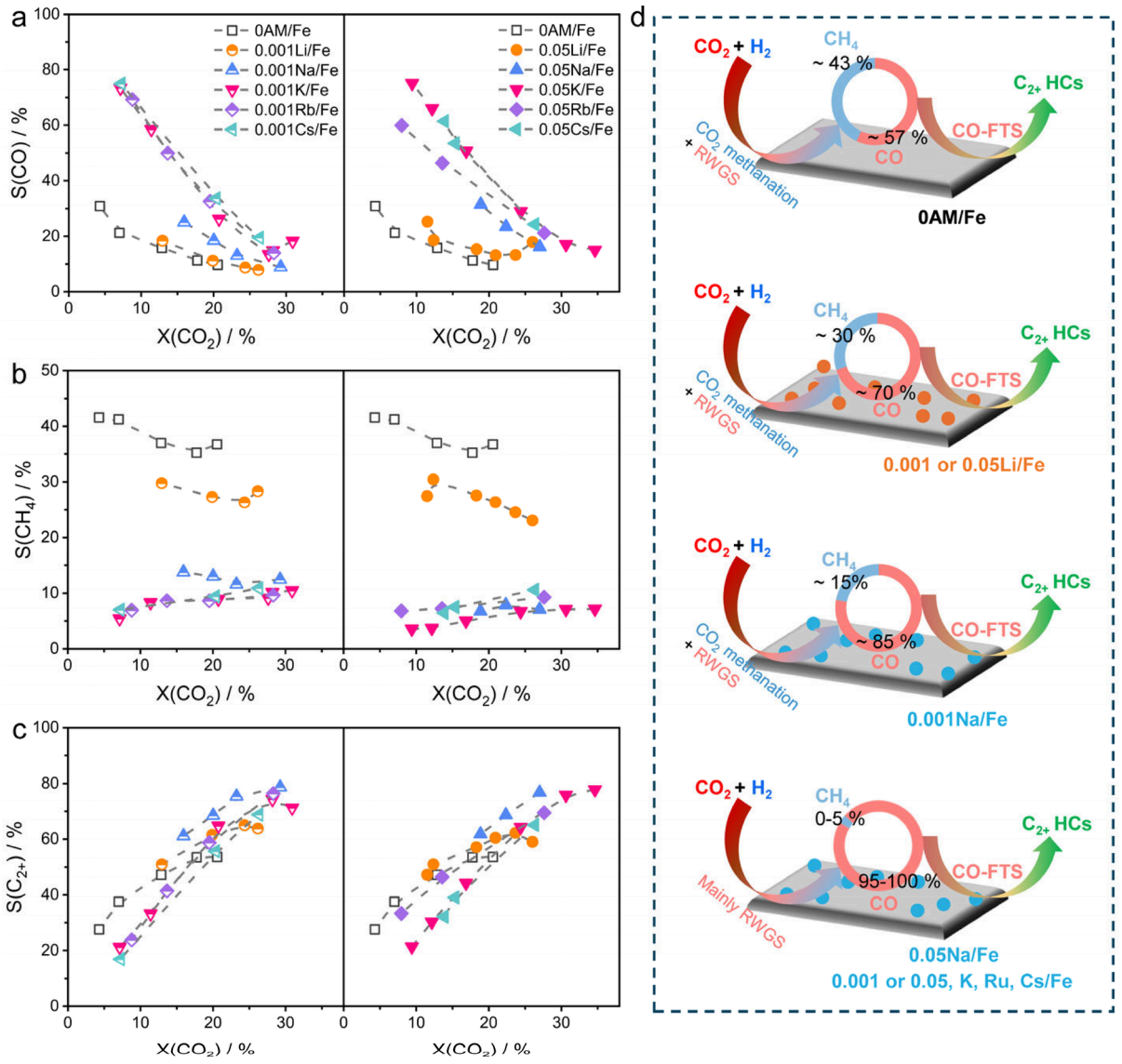

Figure 6. Reaction networks of CO_2-FTS. The dependence of the selectivity to (a) CO, (b) CH_4, and (c) C_{2+}-hydrocarbons on CO_2 conversion over Fe-based catalysts. (d) Graphical representation of the reaction network where the values in cycle represent the selectivity to CH_4 and CO at zero CO_2 conversion. Reproduced with permission from ref 42, which was published under the Creative Commons CC-BY-NC-ND license. Copyright 2022 The Authors.

disappeared for 0.005Li/Fe, and r(CH_4) was considerably lowered for 0.005Na/Fe.

5. MECHANISTIC AND KINETIC ASPECTS OF CO_2-FTS

5.1. Reaction Network of CO_2-FTS

Understanding the product formation scheme and the factors influencing each pathway is a prerequisite for a rational catalyst design. To this end, the selectivity to CO, CH_4, and C_{2+}-hydrocarbons was determined at different levels of CO_2 conversion by varying the space velocity, while holding the temperature and feed composition constant.[19,20,36,42,43] Note, that products with nonzero selectivity at zero conversion are called primary products, while those with zero selectivity are called secondary products. In this context, CO and CH_4 should be formed directly from CO_2 over the M/Fe catalysts (Figure 6a,b).[42] As the CO_2 conversion progresses, the CO selectivity decreases and the selectivity to C_{2+}-hydrocarbons gradually increases from zero (Figure 6c). This means that the primarily formed CO is further hydrogenated to form C_{2+}-hydrocarbons. Based on these results, the overall pathway is described in Figure 6d and Scheme 1, i.e., CO and CH_4 are primary products, while the C_{2+}-hydrocarbons are secondary products formed through CO-FTS. This conclusion does not depend on the promoter content within the investigated range. Meanwhile, additional analysis has suggested that lower olefins are formed directly from CO and then further hydrogenated to the corresponding paraffins resulting in a decrease in their selectivity with increasing CO_2 conversion.[42]

The presence and kind of alkali metal promoter affect the individual contribution of two primary reactions, i.e., CH_4 formation through CO_2 methanation and CO formation through the RWGS reaction, to the overall CO_2 conversion. It is clearly seen that the ratio of the CH_4 selectivity to that of CO at zero CO_2 conversion over the 0AM/Fe catalyst (0.75) is much higher than that of Li/Fe (0.39−0.43), Na/Fe(0.05−0.18), and the catalysts promoted by K, Rb, or Cs (<0.05)

https://doi.org/10.1021/accountsmr.4c00160
Acc. Mater. Res. XXXX, XXX, XXX−XXX

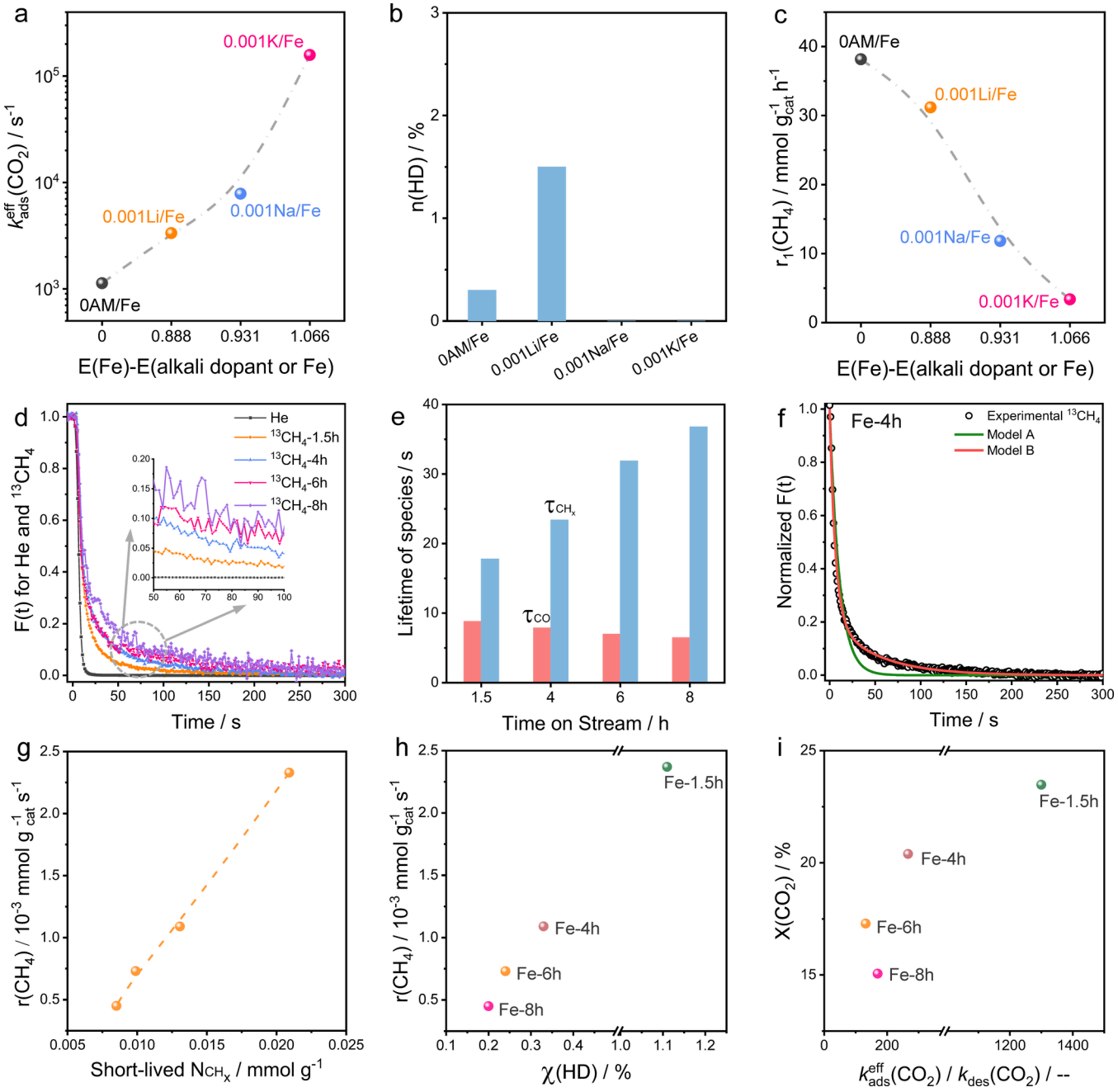

Figure 7. Transient kinetic studies by using the TAP and SSITKA techniques. (a) The rate constants of CO_2 adsorption and (b) HD fraction in H/D exchange experiments using $H_2/D_2/Ar = 1/1/1$ mixture in TAP reactor. (c) The intrinsic rates of CH_4 formation versus the difference in the Allen scale electronegativity of iron and alkali metals. Reproduced with permission from ref 42, which was published under the Creative Commons CC-BY-NC-ND license. Copyright 2022 The Authors. (d) Normalized responses of He and $^{13}CH_4$ after a back-switch from $^{13}CO_2$:H_2:He:Ar to $^{12}CO_2$:H_2:Ar in SSITKA experiments at different times on stream. (e) The lifetime of surface intermediates leading to CO or CH_4 after different times on stream in the CO_2-FTS. (f) The experimental normalized $^{13}CH_4$ transient response collected after 4 h on stream and the fitted data obtained with the single- (Model A) and parallel-pool model (Model B). The rate of CH_4 formation versus (g) the number of short-lived intermediates leading to CH_4 and (h) HD fractions determined by H/D exchange experiments. (i) CO_2 conversion versus the equilibrium constant of the CO_2 adsorption. Reproduced with permission from ref 48. Copyright 2023 American Chemical Society.

(Figure 6). Therefore, the presence of alkali promoters suppresses the CO_2 methanation.

Another important conclusion from Figure 6b relates to the effect of the alkali promoter on the pathways of CH_4 formation. The response of the CH_4 selectivity to the increase in the CO_2 conversion depends on the kind of alkali metal promoter. It increases with rising CO_2 conversion over the K-, Rb-, or Cs-promoted catalysts, suggesting the occurrence of a hydrogenation of CO to CH_4. This process does not occur in CO_2-FTS over the unpromoted or Li- or Na-promoted catalysts. The pathways of CH_4 formation can also be controlled by the defectiveness of Fe_5C_2 formed in situ from unpromoted Fe_2O_3[34] and the particle size of Fe_2O_3 on Fe_2O_3/ZrO_2.[43] An approach to estimate the contribution of CO and CO_2 hydrogenation to the overall CH_4 formation has been developed in our recent study.[44]

https://doi.org/10.1021/accountsmr.4c00160
Acc. Mater. Res. XXXX, XXX, XXX−XXX

The former reaction predominates in the CO_2-FTS over Rb- or Cs-doped catalysts.

In contrast to the above studies, Fedorov et al.[45] suggested that C_{2+}-hydrocarbons can be formed over Fe-K and Fe-K-Mn without the involvement of gas-phase CO. This conclusion was reached because about 30% selectivity to C_{2+}-hydrocarbons could be obtained when extrapolated to zero CO_2 conversion. It has been suggested that some iron carbides can directly hydrogenate CO_2 to form C_{2+}-hydrocarbons. However, no mechanistic concept explaining C−C bond coupling with CO_2 was suggested. Further studies are needed to validate the direct pathway of C_{2+}-hydrocarbons formation from CO_2 and to check if it can help to hinder the undesired CO_2 hydrogenation to CH_4.

In addition to establishing the global network of product formation in CO_2-FTS, it is of fundamental importance to elucidate the activation/evolution of reactants/intermediates at the molecular level, with the goal of fully mapping the catalytic functions of the active phase/species. Transient techniques, in particular, the temporal analysis of products (TAP) reactor operating with a submillisecond resolution,[46] allow the analysis of the activation of feed components and reaction products. The derived mechanistic and kinetic aspects are strongly related to the catalytic performance of the catalysts studied, as demonstrated in, e.g., CH_4 oxidation and CO-FTS,[46] although the TAP reactor operates in vacuum. The abundance and lifetime of surface intermediates leading to a certain gas-phase product can be determined by steady-state isotopic transient kinetic analysis (SSITKA).[47] These methods have been used to distinguish the reactivity of active phases in differently prepared catalysts,[20,34] to reveal the fundamentals behind the promoting effect of alkali metal promoters,[42,44] and to provide kinetic information in the process of catalyst deactivation as described below.[48]

5.2. Fundamentals and Applications of Metal Promotion for Fe-Based Catalysts in CO_2-FTS

Based on a quantitative microkinetic analysis of CO_2 activation over bare Fe_2O_3 and its counterparts promoted with an alkali metal in the TAP reactor,[42] the formation of adsorbed CO and O species proceeds in two steps including reversible non-dissociative CO_2 adsorption and reversible dissociation of adsorbed CO_2. The presence of alkali metal promoter was found to increase the rate constant of CO_2 adsorption which was positively correlated with the difference between the electronegativity of Fe and alkali metal (Figure 7a). A similar trend was observed for the constant of the dissociation rate of adsorbed CO_2. H/D exchange experiments in the TAP reactor showed that the activation of H_2, i.e., the formation of surface H species, was strongly inhibited on iron carbides with the presence of Na or K (Figure 7b). Therefore, alkali metal promoters directly affect the surface ratio of C-containing species to H-containing species, resulting in a lower intrinsic CH_4 formation rate but favoring C−C coupling reactions leading to higher hydrocarbons (Figure 7c).

In contrast to the extensively studied alkali metal promoters for Fe-based catalysts, the promotion effects induced by transition metals are still far from being satisfactorily understood because the latter promoters are typically combined with the former promoters, making it difficult to understand their role. Limited studies using individual transition metals have focused on Co and Mn. The former enhances the degree of CO_2 conversion and the selectivity to C_{2+}-hydrocarbons when the Co/(Fe+Co) atomic ratio is between 0.10 and 0.17.[49] Higher Co content led to a strong increase in the CH_4 selectivity. An appropriate amount of Mn in Fe-based catalysts with a Mn/Fe molar ratio of 0.05 could reduce the selectivity to CH_4 from 49% to 29% compared to a Mn-free reference material due to changes in catalyst basicity.[50] However, the participation of Mn-containing species in catalyst restructuring and their effects on the performance of Fe_xC_y are unclear.

Through harnessing the promotional effects of metals in Fe-based catalysts, product distribution in CO_2-FTS could be further controlled to maximize the selectivity to high-value added products with specifically defined carbon numbers, e.g., jet fuel (C_8−C_{16}),[51] linear high carbon α-olefins (C > 4),[52] and higher alcohols (C > 2),[53−55] besides lower (C_2−C_4) olefins and liquid fuels (C_{5+}). The combination of Na or K with Zn or Mn seems to be decisive for the catalyst performance. For example, the proportion of linear α-olefins in total C_{4+}-alkenes was 85.9% for Na-promoted Fe_5C_2-ZnO catalysts.[52] Besides Cu-modified traditional FTS catalysts that have been used in the synthesis of higher alcohols from CO_2,[53] the approach of sodium-sulfate comodification was developed to regulate the electronic properties of active Fe-containing phases with balanced capabilities toward dissociative and nondissociative CO activation.[54] Gao et al.[55] reported a $ZnFe_2O_4$/Fe-Zn-Na composite catalyst with an exceptional $C_{3+}OH$ yield of 5.3% that was attributed to the facile coupling between CH_2 and CHO species at the interfacial sites between $ZnFe_2O_4$ and Fe_5C_2.

5.3. Origins of Catalyst Deactivation

Catalyst deactivation is the main challenge in the development of CO/CO_2-FTS catalysts and, thus, elucidating the mechanism of catalyst deactivation has always been a central topic in CO-FTS studies over the past decades.[56−58] Extensive studies by Niemantsverdriet et al.[59] on CO-FTS over Co-based FTS catalysts developed by Sasol have shown that carbon deposition and/or sintering of metallic Co species, rather than metal oxidation are the main reason(s) for catalyst deactivation. Relevant studies dealing with the deactivation mechanisms of Fe-based catalysts in FTS with CO or CO_2, especially for the latter, are relatively scarce and vary widely in their conclusions. Deactivation is generally attributed to oxidation of iron carbides by CO_2/H_2O, formation of inactive carbonaceous deposits, and/or Fe_xC_y sintering.[56−58]

Combining in situ XRD, XPS, and Raman spectroscopy, our recent study did not find any reoxidation of Fe_xC_y up to 60 h on CO_2-FTS stream at ambient pressure but confirmed the deactivation mechanism by carbon deposition.[48] The SSITKA method was instrumental in understanding how the overall number (N_i) and lifetime (τ_i) of surface intermediates leading to gas-phase CO and CH_4 change during catalyst deactivation. The SSITKA experiments were performed after different times on stream (TOS) via periodically replacing $^{12}CO_2$:H_2:Ar (1:11:7) with $^{13}CO_2$:H_2:He:Ar (1:11:0.5:6.5). To determine the concentration of reversibly adsorbed CO_2 species after different times on the CO_2-FTS stream, we analyzed the normalized transients of He and $^{13}CO_2$ collected during a switch from $^{13}CO_2$:H_2:He:Ar = 1:11:0.5:6.5 to $^{12}CO_2$:H_2:Ar = 1:11:7. In general, the $^{13}CO_2$ transient response overlapped that of He, suggesting a low coverage of molecularly adsorbed CO_2 species. The N_{CHx} and N_{CO}, as well as τ_{CHx} and τ_{CO}, were determined from the normalized transient of $^{13}CH_4$ (Figure 7d) and ^{13}CO considering the inert reference He. Although both N_{CHx} and N_{CO} decrease with rising TOS, the trends of τ_{CHx} and τ_{CO} do not

https://doi.org/10.1021/accountsmr.4c00160
Acc. Mater. Res. XXXX, XXX, XXX−XXX

match each other (Figure 7e). This suggests that CO and CH_4 are produced at different sites.

To verify the heterogeneity of the sites producing CH_4, the $^{13}CH_4$ transients were fitted by models considering single (one kind of site) or parallel (two different sites) carbon pools (Figure 7f). The transients could be well described by the parallel-pool model, indicating that CH_4 formation involves at least two kinds of carbon pools with different lifetimes. The fitting results showed that the number of short-lived intermediates (high reactivity) decreases gradually with the TOS, which also explains why the overall τ_{CHx} increases with the TOS (Figure 7e). The short-lived intermediates are responsible for the production of CH_4, leading to the linear correlation between their number and the CH_4 formation rate (Figure 7g). Due to the buildup of carbon deposits, the activation of CO_2 and H_2 was hindered as demonstrated by CO_2 pulse and H/D exchange experiments with spent catalysts collected after different TOS. As a result, the rates of CO_2 consumption and CH_4 formation decreased (Figure 7h,i).

Although our studies discussed above at ambient pressure identified carbon formation as the main reason for the activity/selectivity changes in CO_2-FTS over Fe-based catalysts with TOS, the oxidation of iron carbides cannot be excluded under industrially relevant conditions where the oxidation potential of in situ formed water could be stronger due to its higher partial pressure. Thus, both experimental (preferably under operando conditions) and theoretical studies are urgently needed to improve the knowledge of the deactivation mechanisms of Fe-based catalysts in this promising process.

6. SUMMARY AND OUTLOOK

Fe-based catalysts still suffer from high selectivity to CH_4 in CO_2-FTS. Knowledge of the structure−activity-selectivity relationships is key to targeted catalyst design. In this Account, we have demonstrated the potential of combining data science, controllable synthesis of well-defined $Fe_xO_yC_z$ materials, in situ/operando characterization techniques, and kinetic studies to derive mechanistic and kinetic insights into catalyst dynamics and its impact on product formation to control product selectivity in CO_2-FTS. These complementary studies allowed us to revisit several long-debated topics in the field, such as the promoting effects of alkali metal, the mechanisms of catalyst deactivation, and the spatial distribution of steady-state Fe-containing phase in the catalyst bed. The derived fundamental knowledge was used to propose synthesis-property-function relationships to improve the selectivity to C_{2+}-hydrocarbons and to suppress CH_4 formation. The results and approaches may also provide inspiration to other researchers working with Fe-based catalysts, e.g., in CO-FTS or NH_3 synthesis. The introduced spatially resolved analysis of catalyst composition and gas-phase product formation can be applied to any heterogeneous reaction.

Additionally, bifunctional metal oxide-zeolite (also known as OX-ZEO) catalysts, originally proposed by the groups of Bao[60] and Wang[61] for syngas conversion, have been applied to CO_2 hydrogenation, aiming to selectively produce lower olefins or aromatics.[62−64] Unlike CO_2-FTS over Fe-based catalysts where CO formed from CO_2 is hydrogenated to higher hydrocarbons, OX-ZEO catalysts based on In_2O_3, ZnO, or Cr_2O_3 hydrogenate CO_2 to methanol and dimethyl.[62] These products are further converted into target hydrocarbons through methanol-to-olefins (MTO over SAPO-34 zeolite) or methanol-to-aromatics (MTA over ZSM-5 zeolite) processes. However, the insufficient hydrogenation ability of the OX-ZEO catalysts results in inferior levels of CO_2 conversion compared to those of Fe-based catalysts. Simultaneously, the relatively high selectivity to CO (>45%) in the course of CO_2 conversion to methanol limits the yield of lower olefins (below 7−10%) and therefore hinders the industrial application of OX-ZEO systems for CO_2 hydrogenation.[65] Further, the effective integration of metal oxide and zeolite requires precise control of the proximity between them, which increases the operational complexity. Nevertheless, further research efforts are needed to understand the effects of the properties of metal oxides (e.g., their defective structure) and zeolites (e.g., their acidic properties) on the mechanisms involved in CO_2 hydrogenation over OX-ZEO systems, targeting to optimize product distribution and minimize the formation of CO.

Finally, we have also identified the following research areas pertaining to the development of CO_2/CO-FTS catalysts that may be used in industry.

(i) The role of alkali metal promoters for improving C_{2+}-selectivity in CO_2-FTS should be further elucidated. The promoters are simply suggested to influence the electronic properties of iron in iron carbides. Detailed studies demonstrating the direct involvement of species/phases containing an alkali metal promoter in CO_2 conversion are still lacking. However, computational studies of CO-FTS predict that K_2O can stabilize the high-index facets of Fe and therefore affect geometric properties of active phase.[66] Such studies on CO_2-FTS have not been performed to check if alkali metal act as a structural promotor for iron carbide phase(s).

(ii) An important but still unknown feature of promoted Fe-based catalysts is the location and chemical state of metal(oxides) promoters under different conditions such as catalyst activation, reaction, and deactivation. To fill this gap, in situ/operando characterization studies using cells like catalytic reactors are urgently needed. The methods should allow high spatial and temporal resolution. This is also applicable to NH_3 synthesis.

(iii) Since the concentration of Fe_xC_y decreases downstream of the catalyst bed and the efficiency of CO_2 hydrogenation to C_{2+}-hydrocarbons decreases accordingly, it is important to understand the factors (e.g., initial phase composition or morphology, redox properties, and kind of promoter) that influence reaction-induced structural changes of iron carbides. To this end, the controllable synthesis of active Fe_xC_y ex situ or in situ is a major challenge that deserves dedicated studies in the future.

(iv) Reaction intermediates involved in CO_2-FTS and their reactivity are other less-discussed topics in the literature. SSITKA tests coupled with infrared spectroscopy may be useful to detect the reaction intermediates and simultaneously determine their lifetime. Due to the dark color of Fe-based catalysts, the sensitivity of the spectrometers should be improved.

(v) To achieve net negative CO_2 emissions, H_2 used for CO_2 hydrogenation must come from non-CO_2-emitting processes with sustainable energy. To this end, the comprehensive techno-economic analysis and life cycle analysis for the full scenario of carbon capture and utilization may aid in the identification and design of efficient chemical processes for deep decarbonization. In the course of CO_2-FTS, the use of tandem reactors,

https://doi.org/10.1021/accountsmr.4c00160
Acc. Mater. Res. XXXX, XXX, XXX−XXX

separating RWGS and CO-FTS, may break the constraints induced by the different condition requirements of two reactions, likely resulting in an increase in the overall yield of higher hydrocarbons. Furthermore, tandem electrocatalytic−thermocatalytic CO_2 conversion is effective to produce C_3-oxygenates and valuable carbon nanofibers.[67,68] This approach may provide new opportunities for the applications of renewable electricity and facilitate the development of decentralized CO_2 utilization.

AUTHOR INFORMATION

Corresponding Authors

Qingxin Yang − *Leibniz-Institut für Katalyse e. V., 18059 Rostock, Germany*; orcid.org/0000-0001-7073-8703; Email: yangqi@ethz.ch

Evgenii V. Kondratenko − *Leibniz-Institut für Katalyse e. V., 18059 Rostock, Germany*; orcid.org/0000-0003-0431-6937; Email: Evgenii.Kondratenko@catalysis.de

Complete contact information is available at: https://pubs.acs.org/10.1021/accountsmr.4c00160

Author Contributions

All authors have given approval to the final version of the manuscript.

Notes

The authors declare no competing financial interest.

Biographies

Qingxin Yang obtained his PhD under the supervision of Prof. E.V. Kondratenko at Leibniz-Institut für Katalyse (LIKAT Rostock, Germany) in 2022. His research activities have focused on investigating the fundamental aspects of CO_2 hydrogenation and NH_3 oxidation over supported or bulk heterogeneous catalysts, contributing to the establishment of synthesis−property−performance relationships relevant for chemical transformation and energy transition.

Evgenii V. Kondratenko graduated from Novosibirsk State University in 1991 and received his PhD in 1995. In 1997, he was awarded an Alexander von Humboldt Foundation fellowship at the Institute for Applied Chemistry Berlin-Adlershof (group of Prof. Baerns). In 2007, he received his habilitation degree from the Technical University Berlin. Since 2020, he has been a Professor at the University of Rostock. He is currently the head of the department "Advanced methods for applied catalysis" at LIKAT. His research focuses are the development and understanding of catalysts for valorization of C_1−C_4 alkanes, CO_2, and NH_3 as well as reactor engineering concepts.

ACKNOWLEDGMENTS

This work was funded by the Deutsche Forschungsgemeinschaft (DFG) under the priority program SPP2080 "Catalysts and reactors under dynamic conditions for energy storage and conversion" (grant nos. KO 2261/10-1, KO 2261/10-2). We thank the colleagues in departments of "Advanced Methods for Applied Catalysis", "Catalyst Discovery and Reaction Engineering", and "Analytics" at Leibniz-Institut für Katalyse for the assistance and discussion during the implementation of SPP2080 project.

REFERENCES

(1) Bolm, C.; Legros, J.; Le Paih, J.; Zani, L. Iron-Catalyzed Reactions in Organic Synthesis. *Chem. Rev.* **2004**, *104*, 6217−6254.

(2) Torres Galvis, H. M.; Bitter, J. H.; Khare, C. B.; Ruitenbeek, M.; Dugulan, A. I.; de Jong, K. P. Supported iron nanoparticles as catalysts for sustainable production of lower olefins. *Science* **2012**, *335*, 835−838.

(3) Hattori, M.; Okuyama, N.; Kurosawa, H.; Hara, M. Low-Temperature Ammonia Synthesis on Iron Catalyst with an Electron Donor. *J. Am. Chem. Soc.* **2023**, *145*, 7888−7897.

(4) Zecchina, A.; Rivallan, M.; Berlier, G.; Lamberti, C.; Ricchiardi, G. Structure and nuclearity of active sites in Fe-zeolites: comparison with iron sites in enzymes and homogeneous catalysts. *Phys. Chem. Chem. Phys.* **2007**, *9*, 3483−3499.

(5) Theofanidis, S. A.; Galvita, V. V.; Konstantopoulos, C.; Poelman, H.; Marin, G. B. Fe-Based Nano-Materials in Catalysis. *Materials* **2018**, *11*, 831.

(6) De, S.; Dokania, A.; Ramirez, A.; Gascon, J. Advances in the design of heterogeneous catalysts and thermocatalytic processes for CO_2 utilization. *ACS Catal.* **2020**, *10*, 14147−14185.

(7) Wei, J.; Yao, R.; Han, Y.; Ge, Q.; Sun, J. Towards the development of the emerging process of CO_2 heterogenous hydrogenation into high-value unsaturated heavy hydrocarbons. *Chem. Soc. Rev.* **2021**, *50*, 10764−10805.

(8) Visconti, C. G.; Martinelli, M.; Falbo, L.; Fratalocchi, L.; Lietti, L. CO_2 hydrogenation to hydrocarbons over Co and Fe-based Fischer−Tropsch catalysts. *Catal. Today* **2016**, *277*, 161−170.

(9) Wang, W.; Wang, S. P.; Ma, X. B.; Gong, J. L. Recent advances in catalytic hydrogenation of carbon dioxide. *Chem. Soc. Rev.* **2011**, *40*, 3703−3727.

(10) Arinchtein, A.; Ye, M.-Y.; Yang, Q.; Kreyenschulte, C.; Wagner, A.; Frisch, M.; Brückner, A.; Kondratenko, E.; Kraehnert, R. Dynamics of reaction-induced changes of model-type iron oxide phases in the CO_2-Fischer−Tropsch-synthesis. *ChemCatChem.* **2022**, *14*, No. e202200240.

(11) Ding, X.; Zhu, M.; Sun, B.; Yang, Z.; Han, Y.-F. An Overview on Dynamic Phase Transformation and Surface Reconstruction of Iron Catalysts for Catalytic Hydrogenation of CO_x for Hydrocarbons. *ACS Catal.* **2024**, *14*, 6137−6168.

(12) Kirchner, J.; Baysal, Z.; Kureti, S. Activity and structural changes of Fe-based catalysts during CO_2 hydrogenation towards CH_4-A mini review. *ChemCatChem.* **2020**, *12*, 981−988.

(13) Toyao, T.; Maeno, Z.; Takakusagi, S.; Kamachi, T.; Takigawa, I.; Shimizu, K.-i. Machine Learning for Catalysis Informatics: Recent Applications and Prospects. *ACS Catal.* **2020**, *10*, 2260−2297.

(14) Marshall, C. P.; Schumann, J.; Trunschke, A. Achieving Digital Catalysis: Strategies for Data Acquisition, Storage and Use. *Angew. Chem., Int. Ed.* **2023**, *62*, No. e202302971.

(15) Zavyalova, U.; Holena, M.; Schlögl, R.; Baerns, M. Statistical Analysis of Past Catalytic Data on Oxidative Methane Coupling for New Insights into the Composition of High-Performance Catalysts. *ChemCatChem.* **2011**, *3*, 1935−1947.

(16) Yang, Q.; Skrypnik, A.; Matvienko, A.; Lund, H.; Holena, M.; Kondratenko, E. V. Revealing property-performance relationships for efficient CO_2 hydrogenation to higher hydrocarbons over Fe-based catalysts: Statistical analysis of literature data and its experimental validation. *Appl. Catal., B* **2021**, *282*, 119554.

(17) Fedorov, A.; Linke, D. Data analysis of CO_2 hydrogenation catalysts for hydrocarbon production. *J. CO2 Util.* **2022**, *61*, 102034.

(18) Featherstone, N. S.; van Steen, E. Meta-analysis of the thermocatalytic hydrogenation of CO_2. *Catal. Today* **2023**, *423*, 113951.

(19) Skrypnik, A. S.; Yang, Q.; Matvienko, A. A.; Bychkov, V. Y.; Tulenin, Y. P.; Lund, H.; Petrov, S. A.; Kraehnert, R.; Arinchtein, A.; Weiss, J.; Brueckner, A.; Kondratenko, E. V. Understanding reaction-induced restructuring of well-defined $Fe_xO_yC_z$ compositions and its effect on CO_2 hydrogenation. *Appl. Catal., B* **2021**, *291*, 120121.

(20) Yang, Q.; Fedorova, E. A.; Petrov, S. A.; Weiss, J.; Lund, H.; Skrypnik, A. S.; Kreyenschulte, C. R.; Bychkov, V. Y.; Matvienko, A. A.; Brueckner, A.; Kondratenko, E. V. Activity and selectivity descriptors

for iron carbides in CO_2 hydrogenation. *Appl. Catal., B* **2023**, *327*, 122450.
(21) Tu, W.; Sun, C.; Zhang, Z.; Liu, W.; Malhi, H. S.; Ma, W.; Zhu, M.; Han, Y.-F. Chemical and structural properties of Na decorated Fe_5C_2-ZnO catalysts during hydrogenation of CO_2 to linear α-olefins. *Appl. Catal., B* **2021**, *298*, 120567.
(22) Fedorov, A.; Graefe, P. A.; Perechodjuk, A.; Rauch, R.; Wohlrab, S.; Linke, D. Development of Fe-based catalysts for CO_2 hydrogenation to higher hydrocarbons for operating in slurry reactor. *Appl. Catal. A-Gen.* **2024**, *680*, 119749.
(23) Torres Galvis, H. M.; Koeken, A. C. J.; Bitter, J. H.; Davidian, T.; Ruitenbeek, M.; Dugulan, A. I.; de Jong, K. P. Effect of precursor on the catalytic performance of supported iron catalysts for the Fischer−Tropsch synthesis of lower olefins. *Catal. Today* **2013**, *215*, 95−102.
(24) Li, Z.; Liu, J.; Shi, R.; Waterhouse, G. I. N.; Wen, X.-D.; Zhang, T. Fe-Based Catalysts for the Direct Photohydrogenation of CO_2 to Value-Added Hydrocarbons. *Adv. Energy Mater.* **2021**, *11*, 2002783.
(25) Huang, J.; Jiang, S.; Wang, M.; Wang, X.; Gao, J.; Song, C. Dynamic Evolution of Fe and Carbon Species over Different ZrO_2 Supports during CO Prereduction and Their Effects on CO_2 Hydrogenation to Light Olefins. *ACS Sustain. Chem. Eng.* **2021**, *9*, 7891−7903.
(26) Schwertmann, U.; Cornell, R. M. *Iron oxides in the laboratory: preparation and characterization*; John Wiley & Sons, 2000.
(27) de Jong, K. P. *Synthesis of solid catalysts*; John Wiley & Sons, 2009.
(28) Munnik, P.; de Jongh, P. E.; de Jong, K. P. Recent Developments in the Synthesis of Supported Catalysts. *Chem. Rev.* **2015**, *115*, 6687−6718.
(29) Barrios, A. J.; Peron, D. V.; Chakkingal, A.; Dugulan, A. I.; Moldovan, S.; Nakouri, K.; Thuriot-Roukos, J.; Wojcieszak, R.; Thybaut, J. W.; Virginie, M.; Khodakov, A. Y. Efficient promoters and reaction paths in the CO_2 hydrogenation to light olefins over zirconia-supported iron catalysts. *ACS Catal.* **2022**, *12*, 3211−3225.
(30) Zhao, B.; Sun, M.; Chen, F.; Shi, Y.; Yu, Y.; Li, X.; Zhang, B. Unveiling the Activity Origin of Iron Nitride as Catalytic Material for Efficient Hydrogenation of CO_2 to C_{2+} Hydrocarbons. *Angew. Chem., Int. Ed.* **2021**, *60*, 4496−4500.
(31) Chen, Y.; Wei, J.; Duyar, M. S.; Ordomsky, V. V.; Khodakov, A. Y.; Liu, J. Carbon-based catalysts for Fischer−Tropsch synthesis. *Chem. Soc. Rev.* **2021**, *50*, 2337−2366.
(32) Ruiz Puigdollers, A.; Schlexer, P.; Tosoni, S.; Pacchioni, G. Increasing Oxide Reducibility: The Role of Metal/Oxide Interfaces in the Formation of Oxygen Vacancies. *ACS Catal.* **2017**, *7*, 6493−6513.
(33) Hermanek, M.; Zboril, R.; Mashlan, M.; Machala, L.; Schneeweiss, O. Thermal behaviour of iron(II) oxalate dihydrate in the atmosphere of its conversion gases. *J. Mater. Chem.* **2006**, *16*, 1273−1280.
(34) Skrypnik, A. S.; Petrov, S. A.; Kondratenko, V. A.; Yang, Q.; Lund, H.; Matvienko, A. A.; Kondratenko, E. V. Descriptors affecting methane selectivity in CO_2 hydrogenation over unpromoted bulk iron(III)-based catalysts. *ACS Catal.* **2022**, *12*, 11355−11368.
(35) Gu, M.; Dai, S.; Qiu, R.; Ford, M. E.; Cao, C.; Wachs, I. E.; Zhu, M. Structure-Activity Relationships of Copper- and Potassium-Modified Iron Oxide Catalysts during Reverse Water-Gas Shift Reaction. *ACS Catal.* **2021**, *11*, 12609−12619.
(36) Albrecht, M.; Rodemerck, U.; Schneider, M.; Bröring, M.; Baabe, D.; Kondratenko, E. V. Unexpectedly efficient CO_2 hydrogenation to higher hydrocarbons over non-doped Fe_2O_3. *Appl. Catal., B* **2017**, *204*, 119−126.
(37) Skrypnik, A. S.; Lund, H.; Yang, Q.; Kondratenko, E. V. Spatial analysis of CO_2 hydrogenation to higher hydrocarbons over alkali-metal promoted iron(II) oxalate-derived catalysts. *Catal. Sci. Technol.* **2023**, *13*, 4353−4359.
(38) Yang, Q.; Lund, H.; Bartling, S.; Krumeich, F.; Skrypnik, A. S.; Kondratenko, E. V. The role of Na for efficient CO_2 hydrogenation to higher hydrocarbons over Fe-based catalysts under externally forced dynamic conditions. *J. Catal.* **2023**, *426*, 126−139.
(39) Birtill, J. J. But will it last until the shutdown? Deciphering catalyst decay! *Catal. Today* **2003**, *81*, 531−545.
(40) Goelden, V.; Linke, D.; Kondratenko, E. V. Investigation of the Enhancing Effect of Solid Cocatalysts on Propene Formation in Ethene/trans-2-Butene Metathesis over MoO_x/SiO_2-Al_2O_3. *ACS Catal.* **2015**, *5*, 7437−7445.
(41) Wollak, B.; Doronkin, D. E.; Espinoza, D.; Sheppard, T.; Korup, O.; Schmidt, M.; Alizadefanaloo, S.; Rosowski, F.; Schroer, C.; Grunwaldt, J. D.; Horn, R. Exploring catalyst dynamics in a fixed bed reactor by correlative operando spatially-resolved structure-activity profiling. *J. Catal.* **2022**, *408*, 372−387.
(42) Yang, Q.; Kondratenko, V. A.; Petrov, S. A.; Doronkin, D. E.; Saraçi, E.; Lund, H.; Arinchtein, A.; Kraehnert, R.; Skrypnik, A. S.; Matvienko, A. A.; Kondratenko, E. V. Identifying performance descriptors in CO_2 hydrogenation over iron-based catalysts promoted with alkali metals. *Angew. Chem., Int. Ed.* **2022**, *61*, No. e202116517.
(43) Zhu, J.; Zhang, G.; Li, W.; Zhang, X.; Ding, F.; Song, C.; Guo, X. Deconvolution of the particle size effect on CO_2 hydrogenation over iron-based catalysts. *ACS Catal.* **2020**, *10*, 7424−7433.
(44) Skrypnik, A. S.; Petrov, S. A.; Kondratenko, V. A.; Yang, Q.; Matvienko, A. A.; Kondratenko, E. V. Spatially resolved analysis of CO_2 hydrogenation to higher hydrocarbons over alkali-metal promoted well-defined $Fe_xO_yC_z$. *J. Catal.* **2023**, *425*, 286−295.
(45) Fedorov, A.; Lund, H.; Kondratenko, V. A.; Kondratenko, E. V.; Linke, D. Elucidating reaction pathways occurring in CO_2 hydrogenation over Fe-based catalysts. *Appl. Catal., B* **2023**, *328*, 122505.
(46) Morgan, K.; Maguire, N.; Fushimi, R.; Gleaves, J.; Goguet, A.; Harold, M.; Kondratenko, E.; Menon, U.; Schuurman, Y.; Yablonsky, G. Forty years of temporal analysis of products. *Catal. Sci. Technol.* **2017**, *7*, 2416−2439.
(47) Shannon, S. L.; Goodwin, J. G., Jr Characterization of catalytic surfaces by isotopic-transient kinetics during steady-state reaction. *Chem. Rev.* **1995**, *95*, 677−695.
(48) Yang, Q.; Kondratenko, V. A.; Skrypnik, A. S.; Lund, H.; Bartling, S.; Weiss, J.; Brückner, A.; Kondratenko, E. V. Understanding of the Fate of α-Fe_2O_3 in CO_2 Hydrogenation through Combined Time-Resolved In Situ Characterization and Microkinetic Analysis. *ACS Catal.* **2023**, *13*, 9064−9077.
(49) Satthawong, R.; Koizumi, N.; Song, C.; Prasassarakich, P. Bimetallic Fe-Co catalysts for CO_2 hydrogenation to higher hydrocarbons. *J. CO2 Util.* **2013**, *3*−*4*, 102−106.
(50) Al-Dossary, M.; Ismail, A. A.; Fierro, J. L. G.; Bouzid, H.; Al-Sayari, S. A. Effect of Mn loading onto MnFeO nanocomposites for the CO_2 hydrogenation reaction. *Appl. Catal., B* **2015**, *165*, 651−660.
(51) Yao, B.; Xiao, T.; Makgae, O. A.; Jie, X.; Gonzalez-Cortes, S.; Guan, S.; Kirkland, A. I.; Dilworth, J. R.; Al-Megren, H. A.; Alshihri, S. M.; Dobson, P. J.; Owen, G. P.; Thomas, J. M.; Edwards, P. P. Transforming carbon dioxide into jet fuel using an organic combustion-synthesized Fe-Mn-K catalyst. *Nat. Commun.* **2020**, *11*, 6395.
(52) Zhang, C.; Cao, C.; Zhang, Y.; Liu, X.; Xu, J.; Zhu, M.; Tu, W.; Han, Y.-F. Unraveling the role of zinc on bimetallic Fe_5C_2-ZnO catalysts for highly selective carbon dioxide hydrogenation to high carbon α-olefins. *ACS Catal.* **2021**, *11*, 2121−2133.
(53) Xu, D.; Ding, M.; Hong, X.; Liu, G.; Tsang, S. C. E. Selective C_{2+} Alcohol Synthesis from Direct CO_2 Hydrogenation over a Cs-Promoted Cu-Fe-Zn Catalyst. *ACS Catal.* **2020**, *10*, 5250−5260.
(54) Yao, R.; Wu, B.; Yu, Y.; Liu, N.; Niu, Q.; Li, C.; Wei, J.; Ge, Q. Regulating the electronic property of iron catalysts for higher alcohols synthesis from CO_2 hydrogenation. *Appl. Catal., B* **2024**, *355*, 124159.
(55) Yang, H.; Wei, Z.; Zhang, J.; Dang, Y.; Li, S.; Bu, X.; Zhou, Z.; Gong, C.; Wang, H.; Li, J.; Liu, Y.; Yang, Y.; Xiao, T.; Liu, C.; Sun, Y.; Gao, P. Tuning the selectivity of CO_2 hydrogenation to alcohols by crystal structure engineering. *Chem.* **2024**, *10*, 2245.
(56) de Smit, E.; Weckhuysen, B. M. The renaissance of iron-based Fischer−Tropsch synthesis: on the multifaceted catalyst deactivation behaviour. *Chem. Soc. Rev.* **2008**, *37*, 2758−2781.
(57) Zhang, Y.; Cao, C.; Zhang, C.; Zhang, Z.; Liu, X.; Yang, Z.; Zhu, M.; Meng, B.; Xu, J.; Han, Y.-F. The study of structure-performance relationship of iron catalyst during a full life cycle for CO_2 hydrogenation. *J. Catal.* **2019**, *378*, 51−62.

https://doi.org/10.1021/accountsmr.4c00160
Acc. Mater. Res. XXXX, XXX, XXX−XXX

(58) Arce-Ramos, J. M.; Li, W.-Q.; Lim, S. H.; Chang, J.; Hashimoto, T.; Kamata, H.; Sullivan, M. B.; Borgna, A.; Chen, L.; Poh, C. K.; Zhang, J. Investigating the deactivation and regeneration mechanism of Fe-based catalysts during CO_2 reduction to chemicals. *Appl. Catal., B* **2024**, *347*, 123794.
(59) van de Loosdrecht, J.; Ciobîcă, I. M.; Gibson, P.; Govender, N. S.; Moodley, D. J.; Saib, A. M.; Weststrate, C. J.; Niemantsverdriet, J. W. Providing Fundamental and Applied Insights into Fischer−Tropsch Catalysis: Sasol-Eindhoven University of Technology Collaboration. *ACS Catal.* **2016**, *6*, 3840−3855.
(60) Jiao, F.; Li, J.; Pan, X.; Xiao, J.; Li, H.; Ma, H.; Wei, M.; Pan, Y.; Zhou, Z.; Li, M.; Miao, S.; Li, J.; Zhu, Y.; Xiao, D.; He, T.; Yang, J.; Qi, F.; Fu, Q.; Bao, X. Selective conversion of syngas to light olefins. *Science* **2016**, *351*, 1065−1068.
(61) Cheng, K.; Gu, B.; Liu, X.; Kang, J.; Zhang, Q.; Wang, Y. Direct and Highly Selective Conversion of Synthesis Gas into Lower Olefins: Design of a Bifunctional Catalyst Combining Methanol Synthesis and Carbon-Carbon Coupling. *Angew. Chem., Int. Ed.* **2016**, *55*, 4725−4728.
(62) Zhou, W.; Cheng, K.; Kang, J.; Zhou, C.; Subramanian, V.; Zhang, Q.; Wang, Y. New horizon in C1 chemistry: breaking the selectivity limitation in transformation of syngas and hydrogenation of CO_2 into hydrocarbon chemicals and fuels. *Chem. Soc. Rev.* **2019**, *48*, 3193−3228.
(63) Ni, Y.; Chen, Z.; Fu, Y.; Liu, Y.; Zhu, W.; Liu, Z. Selective conversion of CO_2 and H_2 into aromatics. *Nat. Commun.* **2018**, *9*, 3457.
(64) Wang, S.; Zhang, L.; Zhang, W.; Wang, P.; Qin, Z.; Yan, W.; Dong, M.; Li, J.; Wang, J.; He, L.; Olsbye, U.; Fan, W. Selective Conversion of CO_2 into Propene and Butene. *Chem.* **2020**, *6*, 3344−3363.
(65) Chernyak, S. A.; Corda, M.; Marinova, M.; Safonova, O. V.; Kondratenko, V. A.; Kondratenko, E. V.; Kolyagin, Y. G.; Cheng, K.; Ordomsky, V. V.; Khodakov, A. Y. Decisive Influence of SAPO-34 Zeolite on Light Olefin Selectivity in Methanol-Meditated CO_2 Hydrogenation over Metal Oxide-Zeolite Catalysts. *ACS Catal.* **2023**, *13*, 14627−14638.
(66) Huo, C.-F.; Li, Y.-W.; Wang, J.; Jiao, H. Insight into CH_4 formation in iron-catalyzed Fischer−Tropsch synthesis. *J. Am. Chem. Soc.* **2009**, *131*, 14713−14721.
(67) Garg, S.; Xie, Z.; Chen, J. G. Tandem reactors and reactions for CO_2 conversion. *Nature Chemical Engineering* **2024**, *1*, 139−148.
(68) Xie, Z.; Huang, E.; Garg, S.; Hwang, S.; Liu, P.; Chen, J. G. CO_2 fixation into carbon nanofibres using electrochemical-thermochemical tandem catalysis. *Nat. Catal.* **2024**, *7*, 98−109.

https://doi.org/10.1021/accountsmr.4c00160
Acc. Mater. Res. XXXX, XXX, XXX−XXX